Journal of Computational Electronics (2025) 24:59
https://doi.org/10.1007/s10825-025-02295-5

# Characteristics of a V-shaped rectenna for 28.3 THz energy harvesting

**Aboubacar Savadogo[1,2] · Thomas Nyachoti Nyangonda[2] · Bernard Odhiambo Aduda[2] · Uli Lemmer[1,3] · Mohamed Hussein[1,4]**

Received: 4 December 2024 / Accepted: 11 February 2025


**Abstract**

A rectenna structure based on a potentially printable V-shaped nanoantenna (VSNA) design is introduced and numerically analyzed. The characteristics of the VSNA structure have been investigated through the electric field enhancement and radiation efficiency used as figures of merit to evaluate its performance. A comparative study has been performed between the VSNA and a conventional dipole THz antenna based on the same dimension constraints. Therefore, the VSNA has shown better and more localized field enhancement at the arm tips. Furthermore, an optimization process has been carried out to maximize the electric field at the resonance frequency (28.3 THz). The suggested design offers more than 300% improvement in electric field confinement compared to a conventional dipole antenna at 28.3 THz. This enhancement is attributed to the tip-to-tip geometry, leading to a highly localized field at the tip. Further, the optimized VSNA design is employed to form a rectenna structure by inserting an ultra-thin insulator layer between the tips of the antenna arms. The reported rectenna structure increases total efficiency from 11 to 26.58%, with a 141% improvement over previously reported work. Beyond the potentialities presented by the proposed design, its simplicity makes it manufacturable for efficient energy harvesting applications. Finally, the metal–insulator–metal (MIM) diode rectification capabilities have been investigated through a quantum mechanical simulator (built on MATLAB software) with aluminum oxide ($Al_2O_3$) as an insulator sandwiched between gold (Au) and silver (Ag). The suggested MIM diode ($Au/Al_2O_3/Ag$) offers a zero–bias responsivity of 0.93 A/W, which is higher than the previous work based on $Al_2O_3$ which was 0.5 A/W.

**Keywords** V-shaped nanoantenna (VSNA) · IR energy harvesting · MIM diode · Antenna efficiency

## 1 Introduction

The sun is the most coveted source among renewable energy sources (RES). One of the devices capable of transforming solar radiation directly into electrical energy is called a photovoltaic (PV) cell. PV cells generally are limited in their spectral response. Most of the conventional PV technologies only harvest a small part of the total solar energy in the visible and near-infrared (IR) spectra (ca. 0.3–2.5 μm), while a significant part is in the higher wavelength region (2.5 μm up to over 10 μm). On the other hand, the Earth's surface and the atmosphere absorb around 80% of the solar energy. Then, it is re-emitted as infrared (IR) radiation in the 7–17 μm spectral range, and the peak of the earth's emissivity is at 28.3 THz or 10.6 μm in terms of wavelengths [1]. This frequency range cannot be harvested using conventional PV panels [2]. The THz range is the electromagnetic (EM) frequency range between IR and millimeter waves [3]. In addition, there is a growing need to harvest this abundant

✉ Aboubacar Savadogo
aboubacar.savadogo@partner.kit.edu

✉ Uli Lemmer
ulrich.lemmer@kit.edu

✉ Mohamed Hussein
mohamed.hussein@kit.edu

[1] Light Technology Institute (LTI), Karlsruhe Institute of Technology (KIT), Kaiserstraße 12, 76131 Karlsruhe, Germany

[2] Department of Physics, University of Nairobi, PO Box 30197, Nairobi, Kenya

[3] Institute of Microstructure Technology (IMT), Karlsruhe Institute of Technology (KIT), Hermann-von-Helmholtz-Platz 1, 76344 Eggenstein-Leopoldshafen, Germany

[4] Department of Physics, Faculty of Science, Ain Shams University, Abbassia, Cairo 11566, Egypt

Published online: 05 March 2025

EM energy as the future Internet-of-Things (IoT) devices will rely on ubiquitous energy sources. To respond to that, researchers are currently working on a system known as rectenna.

A rectenna is composed mainly of a receiving antenna and a coupling rectifier diode. The rectifying circuit converts the collected EM energy received by the antenna into direct current (DC) voltage. As illustrated in Fig. 1a, the arms of the antenna collect the EM waves and deliver an AC current, which is corrected by the rectifier to a useful DC current for a load. The equivalent circuit is depicted in Fig. 1b, in which the antenna is shown as an AC voltage source in series with a resistance ($R_a$), and the diode is presented as a capacitance ($C_d$) in parallel with a dynamic resistance ($R_d$). Therefore, the antenna impedance must correlate with that of the diode for efficient energy harvesting. The concept of rectennas was initially demonstrated in the 1966s by Brown at microwave frequencies. He achieved more than 90% efficiency in his system in the microwave band [4]. Furthermore, many recent studies conducted by researchers on microwave antennas show advances [5] and applications for energy harvesting [6, 7]. The success of rectennas in the RF/microwave regions has inspired the extension of the rectenna concept to THz (IR) and solar optical frequencies. However, the rectification process at THz is complex. The conventional Schottky diodes, effective at microwave frequencies, lack suitability due to low speed, plasma frequency, and high time constant. Therefore, efficient operation in the IR and beyond requires an alternative ultra-fast diode for IR rectennas.

The metal–insulator–metal (MIM) diode emerges as a promising candidate, capitalizing on femtosecond-fast electron tunneling through thin insulators, ensuring rapid

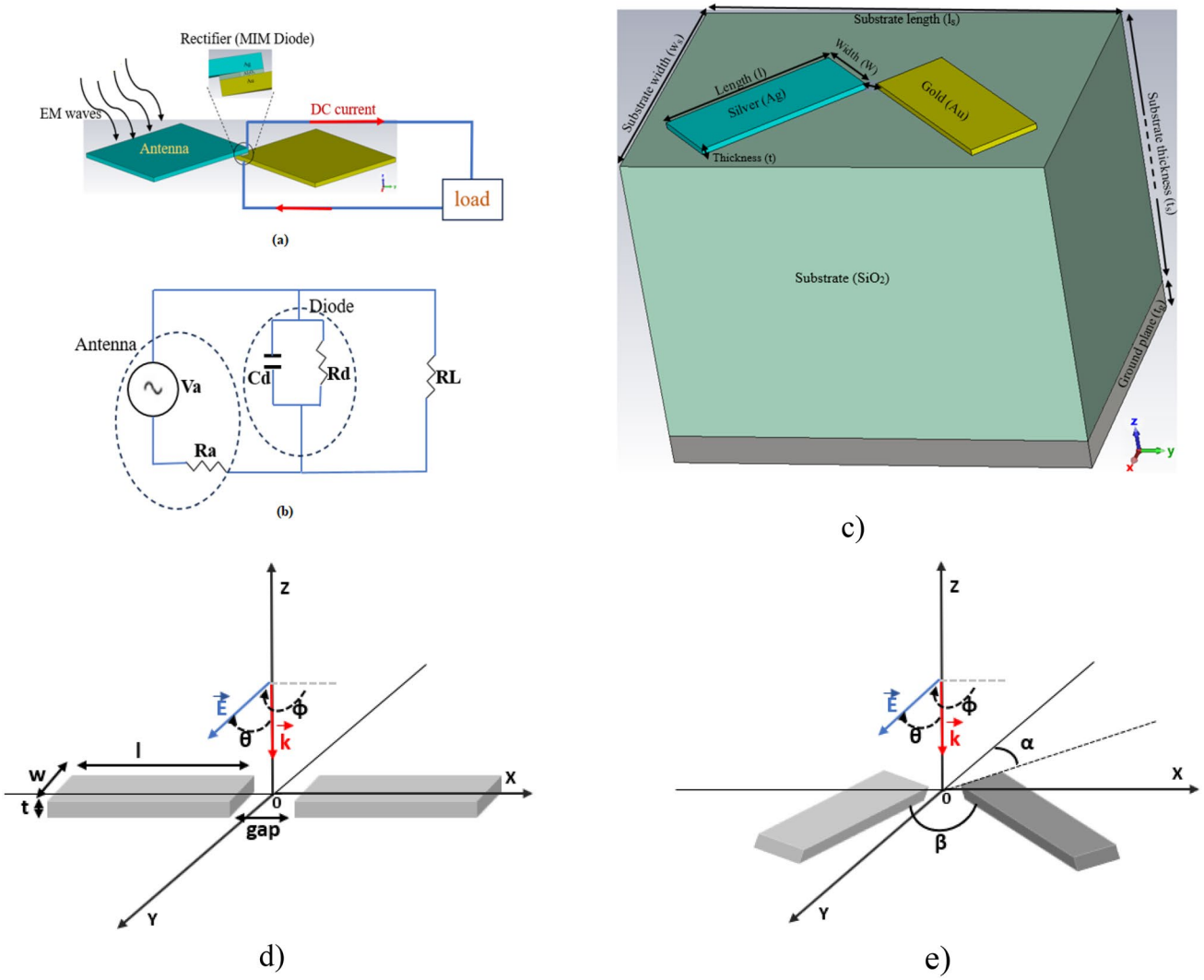


**Fig. 1** **a** Schematic of a typical rectenna device and **b** its equivalent diagram circuit; **c** schematic diagram of the dipole-shaped (VSNA) antenna with substrate and ground plane; **d** conventional dipole, and **e** each arm of dipole tilted relative to *Y*-axis with an angle of $\alpha$ to form the VSNA

rectification [8]. Further, the MIM diodes have zero bias operation, small size, and ultra-fast speed, which is crucial for converting the ultra-fast and small-amplitude input AC signal to DC levels at high frequency. However, achieving optimal rectenna performance involves more than a fast rectification mechanism. It necessitates an impedance matched between the diode and the antenna with a sufficiently low RC time constant [9]. In this regard, several studies have been conducted to enhance the rectenna structure efficiency via several antenna designs, increasing the MIM diode responsivity, and reducing its resistance to improve the coupling with the antenna. In this context, Esfandiari et al. [10] based their study on dipole antenna design coupled with metal-oxide-metal (MOM) to detect IR radiation at 10.6 µm. Gadalla et al. [11] obtained a high zero bias responsivity and low resistance through a rectenna prototype based on a resonant bowtie antenna, which can collect monochromatic IR energy at 28.3 THz. Following this, Kinzel et al. [12] fabricated and tested a slot-antenna-based frequency selective surface (FSS) by employing aluminum oxide($Al_2O_3$) as an insulator sandwich between the two arms of the antenna ($Al/Al_2O_3/Pt$) representing the rectifying structure. This diode showed a zero bias responsivity and resistance of $1.24*10^{-3}$A/W and 124 Ω, respectively. Jayaswal et al. [13] bowtie nanoantenna´s with $Al_2O_3$ as an insulator sandwich between gold and titanium ($Au/Al_2O_3/Ti$) offers a zero bias responsivity of 0.0051 A/W with a resistance of 58 MΩ, proving the possible zero bias rectification of a signal at 28.3 THz by using an MIM diode. Further, Hamied et al. [14] presented Archimedean spiral nanoantenna design with enhanced radiation efficiency and directivity. Yahyaoui et al. [15] presented an antenna design based on an optical log spiral to harvest energy at 10.6 µm. In this investigation, it has been suggested that using an asymmetric diode of $Au/Al_2O_3/Ag$ with that antenna gives the best results after testing different metals (Cu, Cr, Ti, Al, and Ag). The zero bias responsivity achieved is 0.5A/W with a resistance of $0.85*10^{12}$ Ω. Very recently, in the same vein, Amara et al. [16] based their study on a Vivaldi nanoantenna optimized to operate at 28.3 THz employing the same metals (Au and Ag) and insulator($Al_2O_3$). After a parametric study, they obtained a responsivity and resistance of 1 A/W and $4*10^{11}$ Ω at zero bias voltage, respectively. Later, Khouqeer et al. [17] showed the performance of a bowtie antenna and performed a combination of different metals to improve the diode efficiency. It has been demonstrated through their study that the combination showing high responsivity is that of Au and Ag with $ZnO/HfO_2$ as an insulator. However, the zero bias resistance of 173 KΩ obtained remains high, which can reduce the overall efficiency of the rectenna system. Based on the studies mentioned above, it can be deduced that in addition to the insulator and the different metals used, the antenna designs (dipole, bowtie, spiral, and Vivaldi) are also crucial for an efficient rectenna. On the other hand, having a versatile potential antenna design can improve antenna efficiency, leading to an efficient rectenna. In this context, the V-shaped nanoantenna (VSNA) design is full of this potentiality. The VSNA presents a configuration in which two arms of the antenna are close to each other at their apex, thus forming an angle β between them, as depicted in Fig. 1e. Essentially, this configuration allows obtaining a noncolinear set of coupled monopoles. Therefore, it leads to a versatile polarization state for photons where each monopole radiates a polarized electric field parallel to the corresponding axis [18]. This potentiality has been investigated by Rashidi et al. [18], showing how the geometrical parameters and the polarization of the incident plane can influence the resonant frequency of the V-shape antenna. Similarly, Jiao et al. [19] achieved optical focusing by constructing an ultra-thin planar lens with a V-shaped nanoantenna configuration.

Therefore, regarding these potentialities, a V-shaped nanoantenna (VSNA) design derived from the conventional dipole is introduced to enhance rectenna performance. This design enhances and localizes the electric field at the tips compared to a traditional dipole antenna with the same dimension constraints. It reduces the contact from face-to-face to tip-to-tip. A theoretical study has been performed, which showed an electric field improvement of more than 300% compared to a conventional dipole antenna at 28.3 THz. The introduced rectenna based on VSNA offers, by using $Al_2O_3$ as an insulator sandwiched between Au and Ag, an improvement in terms of reducing the zero bias resistance to 33.7 kΩ and an enhanced responsivity to 0.93 A/W. The manuscript is organized as follows: Sect. 2 discusses the design considerations and simulation methodology for the proposed V-shaped nanorectenna. Section 3 presents the simulation results and includes a discussion of their implications. Section 4 focuses on the simulation of the MIM diode and evaluates its performance. Finally, Sect. 5 summarizes the conclusions derived from the study.

## 2 Design consideration and simulation methodology

### 2.1 Structure of the V-shaped nanorectenna

The Computer Simulation Technology (CST)-Microwave Studio software package has been used in this study. This software is based on the 3D full-wave EM field finite integral technique (FIT), which is a consistent discretization scheme for Maxwell's equations. The proposed nanorectenna consists of a V-shaped nanoantenna (VSNA) integrated with a metal–insulator–metal (MIM) diode, as depicted in Fig. 1c. Figure 1c shows the three-dimensional (3D) view of the proposed VSNA, and Fig. 1a presents the VSNA integrated

with a single insulator MIM ($Au/Al_2O_3/Ag$) diode. Figure 1e shows a V-shaped nanoantenna derived from the conventional dipole antenna depicted in Fig. 1d. This antenna consists of two arms that are equal in length, width, and thickness. Each arm has been tilted relative to the Y-axis at an equal angle ($\alpha = 45°$), as shown in Fig. 1e, to create the tip-to-tip facing, which is crucial for electric field enhancement. V-shaped antennas can support both "symmetric" and "antisymmetric" modes [18], and the resonance frequency can significantly shift by changing the polarization of the incident electric field from one to the other [18]. The polarization of the antennas determines the electric field distribution on the nanoantenna and is crucial for energy harvesting applications [1]. Therefore, to assess the field intensity, the proposed VSNA is excited from the top by a 1 V/m (electric field intensity) linearly polarized incident plane wave, with its E-vector parallel to the *X*-axis and propagating normally on the antenna in the Z-axis direction [16, 20, 21].

The VSNA is designed with two metal arms made of gold (Au) and silver (Ag) based on the Drude model (see Sect. 2.2) and characterized by different parametric dimensions as the length($l$), width($w$), metal thickness($t$), and gap($g$) between the arms of the VSNA (Fig. 1(c)). We consider a design where the two arms are placed on a silicon dioxide substrate ($SiO_2$) with dimensions, length($l_s$), width($w_s$), and thickness($t_s$). The choice of substrate for terahertz (THz) applications is critical for the efficient performance of rectenna devices. Substrates with higher dielectric constants can decrease the efficiency due to increased reflection and impedance mismatching [22]. Consequently, $SiO_2$ was selected as the substrate because it has a lower permittivity ($\varepsilon_r = 3.75$) and demonstrates low dielectric loss in the terahertz range. This selection minimizes signal attenuation and enhances the overall efficiency of the device. The substrate is terminated with a perfect electric conductor (PEC) as a back reflector with thickness ($t_g$).

The flow chart of the proposed V-shaped nanoantenna simulated at 28.3 THz with the CST Studio Suite is depicted in Fig. 2.

The proposed V-shaped nanoantenna can be fabricated effectively due to advances in nanotechnology. Therefore, all the dimensions referred to in this paper, including width, length, thickness, and gap, are both producible and controllable. Typically, nanoantennas are manufactured

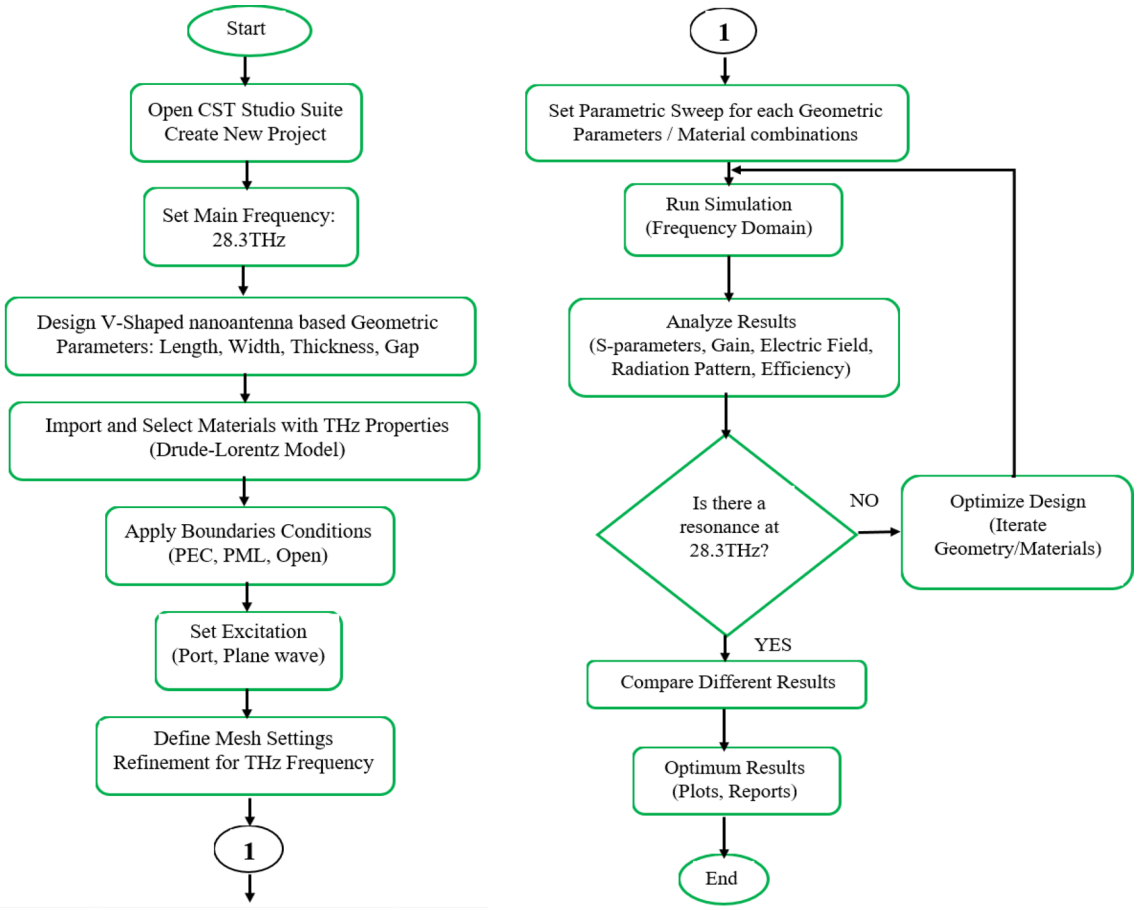


**Fig. 2** Flowchart for the proposed V-shaped nanoantenna simulated at 28.3 THz using CST studio suite

using techniques such as electron-beam lithography (EBL) and focused ion beam (FIB) methods [4, 23]. The EBL technique can achieve patterning with less than 10 nm resolution. In contrast, the maskless FIB technique can produce nanoantennas with sub-5 nm nanopore resolution in solid-state membranes [24]. These fabrication methods were recently used to manufacture nanoantennas with precise and highly controllable parameters [25]. Furthermore, the reported VSNA features a minimum size of 10 nm to ensure compatibility with these techniques and incorporates a larger gap size to simplify the fabrication process.

The second part of this study consists of the design and simulation of the MIM diode that will be used as a rectifier to convert the AC current delivered by the antenna to a usable DC current for a load. Therefore, a quantum mechanical simulator is required and built through MATLAB software to evaluate the performance of a MIM diode and the tunneling characteristics as described in details in [2]. The simulator employs a variant of tunnel barrier characterized by diverse voltage values, utilizing the transfer matrix method [13] to compute the tunneling probability. The simulator calculates the tunneling current by incorporating the probability of tunneling and the Fermi distribution of electrons. The configuration of the barrier is defined by material parameters such as the metals' work function, the electronic affinity of the insulator, and the applied bias voltage. The metal work function (WF) is the minimum energy needed to eject an electron to a point in the vacuum outside a metal surface. The difference between the value of WF and the insulator's electron affinity gives the tunnel barrier height [2, 26].

### 2.2 Material properties used at high frequencies

All the antenna dimensions enumerated above must be optimized to allow the antenna to resonate at wavelengths of 10.6 µm or 28.3 THz based on the dimension constraints mentioned above (Sect. 1). The properties of metals change within the terahertz (THz) frequency range, resulting in their behavior deviating from that of perfect conductors. To address this, the Drude model has been used to describe the material properties of gold and silver in this frequency range [27, 28] and import them into the CST simulator. The variations of the relative permittivity $\varepsilon_r$ versus frequency for silver and gold are given in Fig. 3. The frequency-dependent complex permittivity of metals at the THz range through the Drude model is given in [28]:

$$\varepsilon_r = \varepsilon_1 + j\varepsilon_2 = \varepsilon_\infty - \frac{\omega_p^2}{\omega(\omega + j\omega_\tau)} \tag{1}$$

From Eq. 1, $\varepsilon_1$ and $\varepsilon_2$ can be deducted as following [28]:

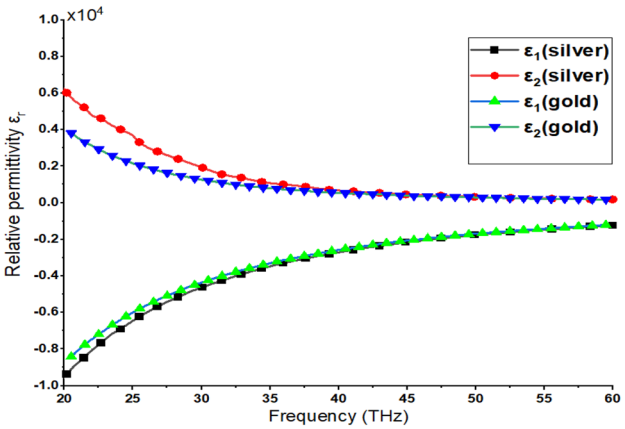


**Fig. 3** Relative permittivity versus frequency for silver and gold

$$\varepsilon_1 = \varepsilon_\infty - \frac{\omega_p^2}{\omega^2 + \omega_\tau^2} \tag{2}$$

$$\varepsilon_2 = \frac{\omega_p^2 \omega_\tau}{\omega^3 + \omega\omega_\tau^2} \tag{3}$$

where $\varepsilon_1$ represents the real part of the permittivity. $\varepsilon_2$ is the imaginary part representing the loss or dissipative factor. $\omega$, $\omega_\tau$ and $\omega_p$ represent the angular frequency, collision frequency and the plasma frequency, respectively.

## 3 Simulation results and discussion

### 3.1 V-shaped nanoantenna (VSNA)

A parametric study has been done to maximize the electric field localized at the arm tips and gap of the nanoantenna. Before studying the main parameters of the proposed V-shaped nanoantenna (VSNA), the effect of the incident plane wave polarization has been investigated. In this study, the normal incident plane wave is colinear to the E-vector and propagating in the direction of the k-vector, as depicted in Fig. 1e and f. Here, the angle $\theta$ is kept constant at 0°, while the angle Φ varies from 0 (corresponding to an *X*-polarized plane wave) to 90° (corresponding to a Y-polarized plane wave). Figure 4a shows the electric field variation versus frequency for linear and circular polarization in normal incident plane wave ($\theta = 0°$ and $\Phi = 0°$). It can be seen from this figure that the proposed VSNA is compatible with linear and circular polarization. However, the circular polarization yields a higher electric field intensity at 28.3 THz. The electric field intensity versus frequency with different electric field polarization angles is shown in

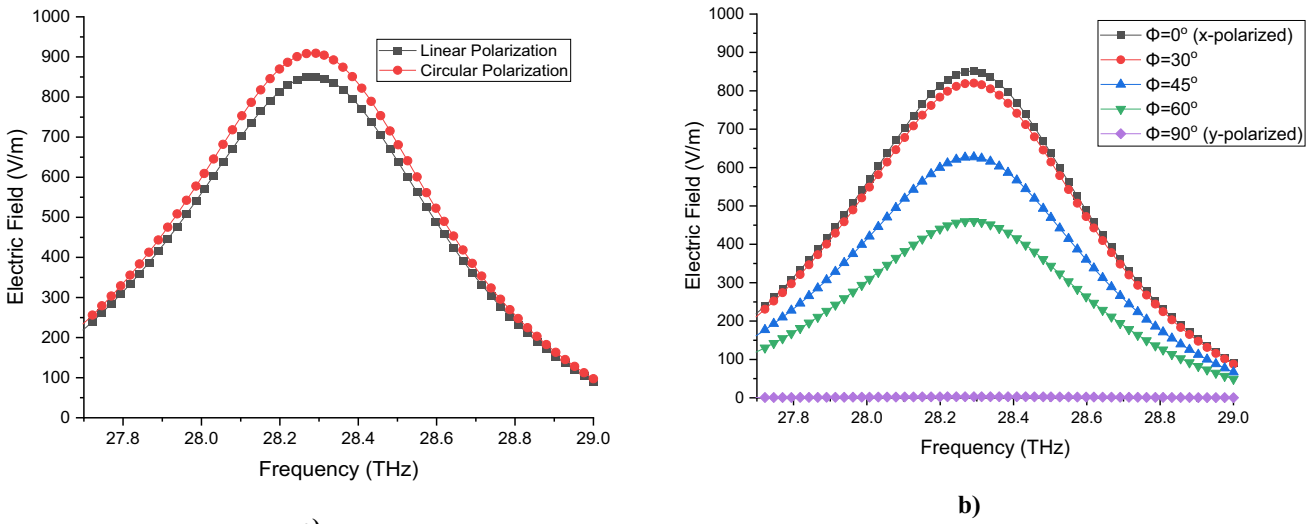


**Fig. 4** **a** The electric field variation versus frequency for linear and circular polarization in normal incident plane wave ($\theta=0$ and $\varphi=0$), **b** for different values of ϕ

Fig. 4b). The maximum electric field intensity is obtained at the V-shaped nanoantenna gap and occurs at 28.3 THz. It decreases when Φ increases from 0 to 90°.

After studying polarization, various simulations were conducted to explore key geometrical parameters: length ($l$), width ($w$), metal thickness ($t$), and gap ($g$). This involved varying one parameter while keeping the others constant to achieve maximum electric field enhancement at 28.3 THz for each. The compiled values were then used to create the diagrams in Figs. 7 and 9, aiding in the selection of optimal values at 28.3 THz. Before that, the effect of the substrate thickness ($t_s$), the nature of the metal, and their combinations on the electric field variation, as well as the comparison between the suggested VSNA and a conventional dipole, are studied. Throughout the study, one of the design parameters varies while the others are kept constant at $l_s=7.14$ µm; $w_s=5.3$ µm; $t_s=42.4$ µm; $t_g=0.005$ µm; $l=2.7$ µm; $w=2.3$ µm; $t=0.1$ µm; and $g=0.01$ µm. All the figures presented below have been plotted under these conditions after obtaining the optimum values. Figure 5 shows the electric field enhancement of the VSNA versus frequency for different thicknesses of the substrate (a) and different metals used (b). Furthermore, a comparison between VSNA and a conventional dipole in electric field enhancement (c) and return loss versus frequency is shown in Fig. 5d. It can be noticed from Fig. 5a that the thickness of the substrate has a significant effect on the electric field variation, which agrees with previous work reported in [17, 29], while the substrate thickness increases from 5.3 to 42.4 µm the electric field increased from 55.33 to 918.62 V/m at 28.3 THz, respectively. Figure 5b shows the electric field localized by the antenna with the variation of antenna arm materials; in this study, one arm material is fixed as gold (Au), and the second arm material is changed. It can be seen from this figure that a combination of silver and gold shows the best result in terms of field enhancement. This can further facilitate the tunneling and enhance the asymmetry for diode integration [17]. The silver shows a better electric field than gold due to its low dissipation factor ($\varepsilon_2$) at 28.3THz. Figure 5c compares the VSNA design and a conventional dipole antenna. It is evident from Fig. 5c that the VSNA has a higher electric field enhancement of 563.03 V/m compared to 129.01 V/m for a conventional dipole, which is equivalent to an improvement of 336%. Indeed, they have been designed with the same length, width, and thickness to have the same volume. It is worth mentioning that the dimension constraints have also been considered to facilitate further fabrication with a costless and high producibility technique [30, 31]. However, each arm of the conventional dipole has been tilted with an angle of α (45°) degree to form tip-to-tip, which causes the group and phase velocity of the surface plasmon waves to reach zero at the tips, leading to a highly localized field at the tips as depicted in Fig. 6. This figure shows the electric field distribution for a conventional dipole (a) versus VSNA (b). The electric field is scattered in the case of the conventional dipole, as depicted in Fig. 6a. In analogy to bowtie nanoantennas, the field enhancement in the gap of the VSNA is higher than that of a conventional dipole due to a larger lightning-rod effect at the apex [32]. We can also notice through Fig. 5d that tilting the conventional dipole arms with an angle of 45° relative to the Y-axis shifts the resonance to the interest frequency, around 28 THz. As for the VSNA, the connection between the two arms is done in a tip-to-tip geometry. Therefore, the plasmon coupling region

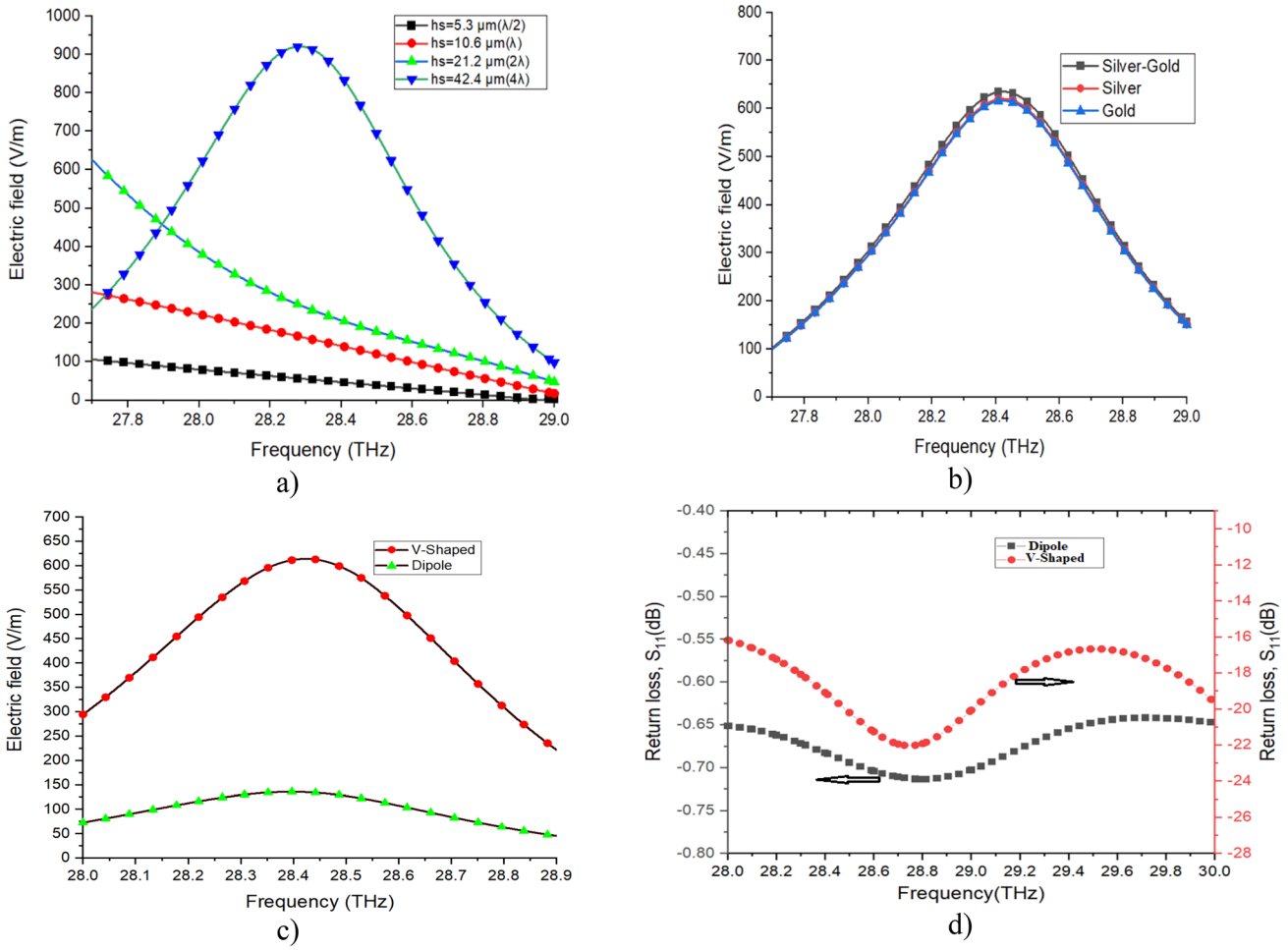


**Fig. 5** Electric field enhancement of V-shaped nanoantenna versus frequency for **a** different thicknesses of the substrate, **b** different metals used; Comparison between V-shaped nanoantenna and conventional dipole in **c** electric field enhancement and **d** return loss versus frequency

is much reduced than in a conventional dipole. The near-field enhancement increases when the arms are closer, displaying an apparent hot spot [33].

In energy harvesting applications, one is interested in increasing the electric field enhancement. Therefore, the following study is dedicated to find the optimum geometrical parameters that offer the highest values of the electric field enhancement at 28.3 THz. Therefore, Fig. 7 summarizes the previous Fig. 5a, b, and c by showing the electric field enhancement as a function of the design parameters. This lets us quickly determine the optimum design values, material nature, and shape for maximum field enhancement at the desired frequency. Therefore, a VSNA with silver and gold as materials for the two arms and a substrate thickness ($SiO_2$) of 42.2 μm are considered for the following sections.

After obtaining the optimum thickness of the substrate and the best combination of metals through a parametric study, this section now deals with the design parameters of the VSNA, such as the gap between the two arms of the antenna, the length, the width, and the metal thickness of each arm of the antenna. To do this, Fig. 8 depicts the electric field variations versus frequency for different parameters of the VSNA. Figure 8a illustrates the effect of variation of the gap size on the collected electric field. As the gap decreases from 50 to 0.5 nm, the electric field enhancement increases from 140 to 17,060 V/m at 28.3 THz. Then, when the tip of each arm of the nanoantenna is very close to each other (very small gap size), the electric field is maximum [33]. This enhancement is attributed to a combination of plasmonic resonance, near-field effects, and increased capacitance, where the electric field enhancement is particularly strong in the near-field region close to the nanoantenna surface. As the gap size decreases, the near-field interactions become more dominant, causing a more significant increase in the local electric field strength. Furthermore, the decrease in gap size increases the capacitance between the metal components of the nanoantenna. This higher capacitance contributes to a more efficient accumulation and concentration

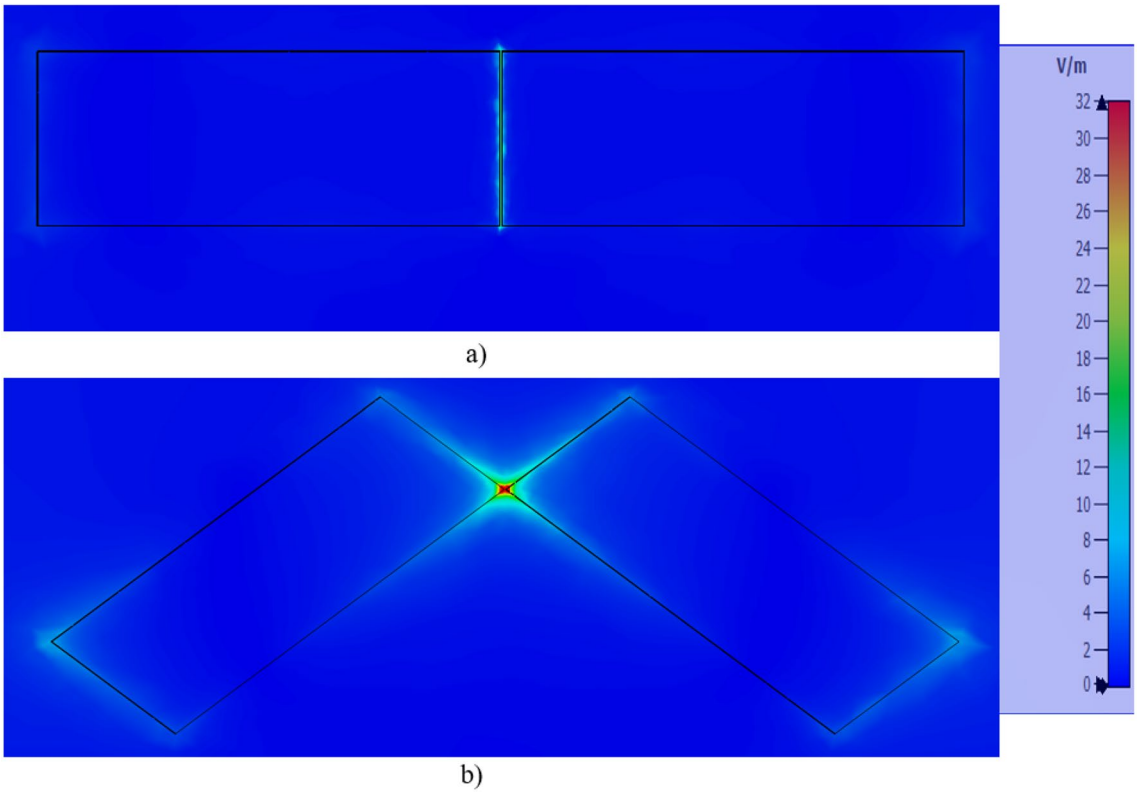


**Fig. 6** Electric field distribution for **a** conventional dipole **b** versus V-shaped nanoantenna

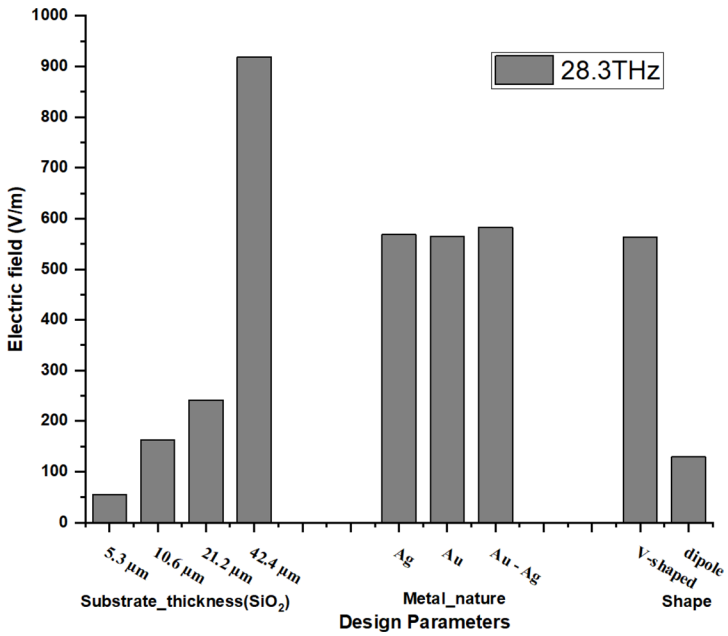


**Fig. 7** Value of the electric field at 28.3 THz for the different designs

of charge, leading to stronger electric fields in the gap. Next, a parametric study is carried out on the antenna width, length, and metal thickness to visualize the impact of these parameters on the value of the electric field. Here, as shown in Fig. 8b, the variation of the width from 1 to 2.3 µm leads to an increase in the electric field. However, the length variation from 2.5 to 3.2 µm only slightly affects the electric field, as we can observe in Fig. 8c. Contrary to the width,

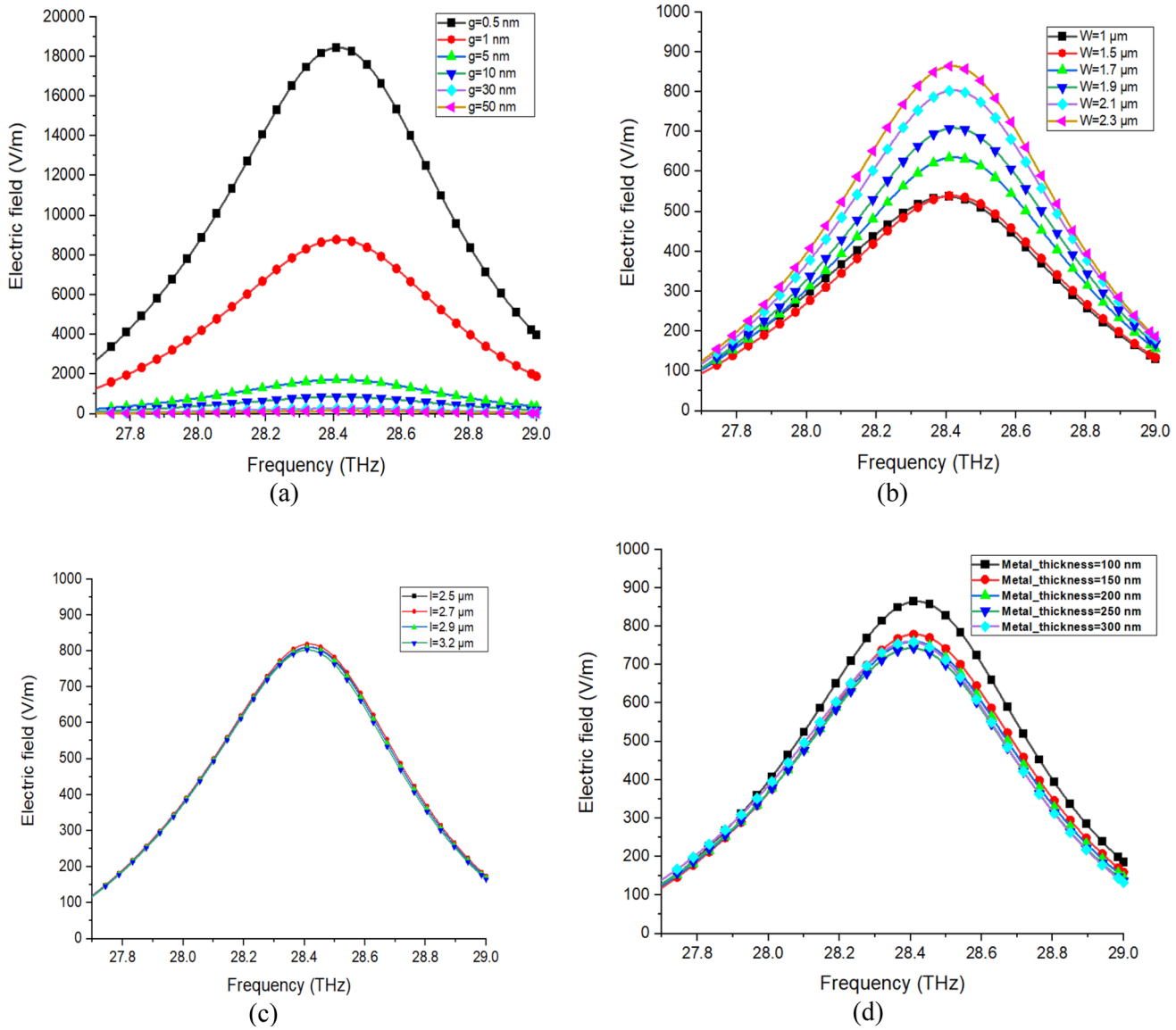


**Fig. 8** Electric field variations versus frequency for the V-shaped nanoantenna: **a** gap variation, **b** length variation, **c** width variation, and **d** metal thickness variation

we observe a decrease in the electric field when the length increases. Therefore, the losses are much more pronounced for the increasing length [21]. Another critical parameter to study is the effect of the antenna thickness on the electric field enhancement. Figure 8d shows this study's numerical results. It can be observed from this figure that the thinner metal thickness shows higher electric field enhancement due to less pronounced field localization for thicker films.

Figure 9 summarizes the results from Fig. 8a, b, c, and d. It presents a diagram of the electric field variation versus different design parameters precisely at 28.3 THz to extract the optimum values of the VSNA parameters for maximum field enhancement. Therefore, the optimum values are 2.7 µm for the length, 2.3 µm for the width, and 0.1 µm for the metal thickness. All these values are summarized in Table 1. Figure 10 shows the field enhancement (a) and the return loss (b) versus frequency with an input impedance of 130 Ohm (Ω) for the optimum VSNA. From Fig. 10a, it can be seen that the maximum field enhancement occurs at the desired frequency of 28.3THz with a value of 918.62 V/m accompanied with a return loss of −15.59 dB. Figure 10b illustrates that the reported VSNA has a return loss of less than −10 dB from 26 to 29 THz. Therefore, we can confirm that the designed antenna has broadband impedance matching and is thus suitable for energy harvesting in the 28.3 THz frequency range.

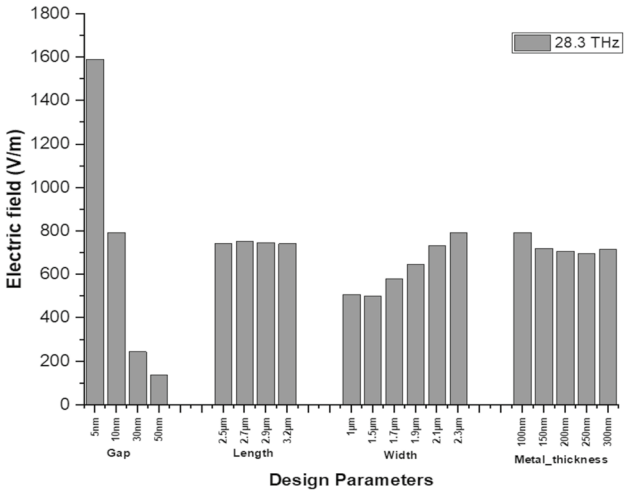


**Fig. 9** The values of electric field versus different design parameters precisely at 28.3 THz

**Table 1** Optimum values for enhancing the electric field at the tips of VSNA

| Design parameters | Optimum values |
|---|---|
| Gap(nm) | 10 nm |
| Length(μm) | 2.7 μm |
| Width(μm) | 2.3 μm |
| Metals | Ag-Au |
| Metal thickness(μm) | 0.1 μm |
| Substrate thickness ($SiO_2$) | 42.4 μm |
| Substrate length | 5.3 μm |
| Substrate width | 7.14 μm |
| Ground plane thickness (PEC) | 0.005 μm |
| Overlap area | $0.06\times0.06$ μm$^2$ (see Sect. 3.2) |
| Insulator thickness ($Al_2O_3$) | 1.5 nm (see Sect. 3.2) |

### 3.2 VSNA rectenna with $Al_2O_3$ insulator

In this part, the VSNA studied in Sect. 3.1 has been combined with $Al_2O_3$ to form a rectenna. Thus, an overlapping VSNA (ovVSNA) with a thin insulator layer ($Al_2O_3$) between the tips of the two arms, as depicted in Fig. 1a, is numerically analyzed. The antenna radiation efficiency $\eta_r$ is given by Eq. (4) [9, 26, 29]:

$$\eta_r = \frac{P_r}{P_{\text{in}}} = \frac{P_r}{P_r + P_{\text{loss}}} \tag{4}$$

where $P_r, P_{\text{in}} and P_{\text{loss}}$ represents the power radiated, power input into the antenna, and the power dissipated in the nano-antenna, respectively.

This section investigates the influence of the integrated insulator thickness and the overlapping area on the electric field enhancement and efficiency of the rectenna system. The results are presented in Fig. 11, which depicts the electric field and radiation efficiency versus frequency for different insulator thicknesses and overlapping areas. The total efficiency and the radiation pattern are also presented. From Fig. 11a and b, the maximum electric field is obtained at around 28.3 THz, and we can notice that the electric field decreases when the insulator's thickness and the VSNA's overlap area increase. However, in Fig. 11c and d, we can observe an increase in the radiation efficiency when these parameters increase. In these figures, it can be noticed that the radiation efficiency of the proposed overlapping structure is high and amounts to about 98%. This is due to the optimization study conducted previously in Sect. 3.1, which aimed to maximize the electric field enhancement at the tip of the VSNA before inserting the insulator, reducing losses in the rectenna system. Indeed, the radiation efficiency of the ovVSNA coupled with the MIM diode inserted between the tips of the two arms of the antenna depends strongly on the nature of the insulator used, its thickness, and the overlapping area. The 3D radiation E-pattern is another important characteristic that indicates the capability of our design to radiate and or receive propagating electromagnetic waves. The resulting radiation pattern of the VSNA with overlapping arms (ovVSNA), including an insulator ($Al_2O_3$) at 28THz, is shown in Fig. 11e. It is observable that the ovVSNA design presents a wide angular reception. Therefore, the total efficiency of our proposed rectenna system at 28.3 THz is 26.58% (Fig. 11(f)) which is more than previous reported works in [13] and [16].

## 4 THz MIM diode simulation and performance determination

The suggested VSNA, including the insulator, forms a MIM ($Au/Al_2O_3/Ag$) diode at its terminals. In this section, the resulting tunneling currents and the efficiencies are calculated based on the properties of the different materials used. The metals Au and Ag work functions are 5.1 and 4.26 eV, respectively [17]. The electron affinity and the dielectric constant at 28 THz of the insulator, $Al_2O_3$ are 4.2 eV and 3.85, respectively [34]. The overlap area is assumed to be square with a thickness of 1.5 nm ($0.06\times0.06\times0.0015$ μm$^3$). These values have been taken from Table 1 and represent the optimum values obtained when simulating the ovVSNA. According to Eqs. 5 and 6, the overlapping area should be small to reduce the diode's capacitance and thus enhance its cut-off frequency. Since the cutoff frequency is inversely proportional to the diode capacitance [1, 4, 17]:

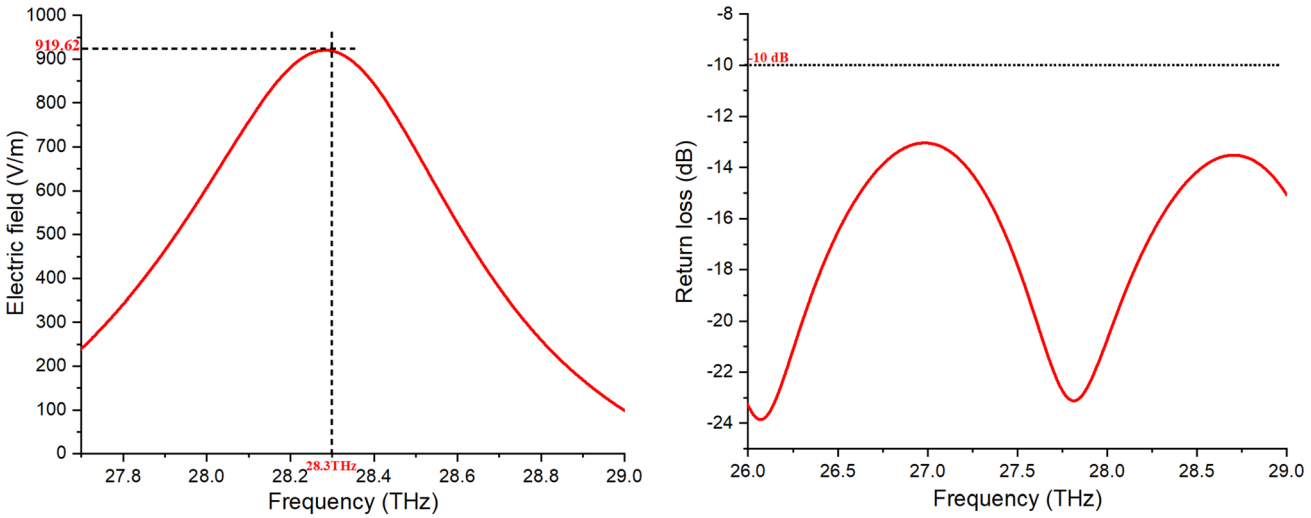


(a) (b)

**Fig. 10** Field enhancement **a** and return loss **b** versus frequency plotted with the optimum design values

$$f_c = \frac{1}{2\pi R_D C_D} \tag{5}$$

$$C_D = \varepsilon_0 \varepsilon_r \frac{A}{d} \tag{6}$$

where $R_D$ and $C_D$ are, respectively, the equivalent resistance and the capacitance of the MIM diode; $\varepsilon_0$ and $\varepsilon_r$ are the dielectric constant of vacuum and relative dielectric constant, respectively; $d$ and A represent the thickness of the dielectric and the overlap area.

The main characteristics used to evaluate the MIM diode's performance are its responsivity, resistance, asymmetry, and nonlinearity [8]. The simulation results are depicted in Fig. 12, representing the *I-V* characteristic (a), the responsivity and the dynamic resistance (b), the asymmetry (c), and the nonlinearity (d) of the MIM ($Au/Al_2O_3/Ag$) diode for different bias voltages ($-0.4$ to $+0.4$). The diode responsivity ($\beta$) is obtained from the *I-V* characteristic through Eq. 7 [2]. It evaluates the capability of the diode to rectify the delivered AC current from the antenna. To achieve rectification, the diode must have an asymmetrical *I-V* characteristic [35]. The resistance is evaluated using Eq. 8, and the asymmetry and the nonlinearity, respectively, are determined with Eqs. 9 and 10 [26, 36].

$$\beta = \frac{1}{2} \frac{\frac{d^2 I}{dV^2}}{\frac{dI}{dV}} \tag{7}$$

$$R_D = \frac{dV}{dI} \tag{8}$$

$$A = \left| \frac{I(+V)}{I(-V)} \right| \tag{9}$$

$$\mathrm{NL} = \left( \frac{dI}{dV} \right) \frac{V}{I} \tag{10}$$

At high frequencies, for IR energy harvesting, the diode should be able to work without any bias voltage [37]. At zero bias, the dynamic resistance and responsivity are 33.7 kΩ and 0.93 A/W, respectively. This shows the diode's capability to rectify the incoming AC-to-DC current without applying any bias. An enhancement in the figures of merit can be noticed. Using Au and Ag as antenna arms exhibit highly different work functions, thus facilitating tunneling without applied bias voltages. The asymmetry and nonlinearity values are slightly lower than in Ref.[35], where more than one insulator layer was used. The number of insulator layers used determine the *I-V* characteristics' behavior due to the barrier height change at each interface [35]. Table 2 compares our work and previous work based on antenna design and the figures of merit of MIM diodes at 28.3THz using $Al_2O_3$ as an insulator.

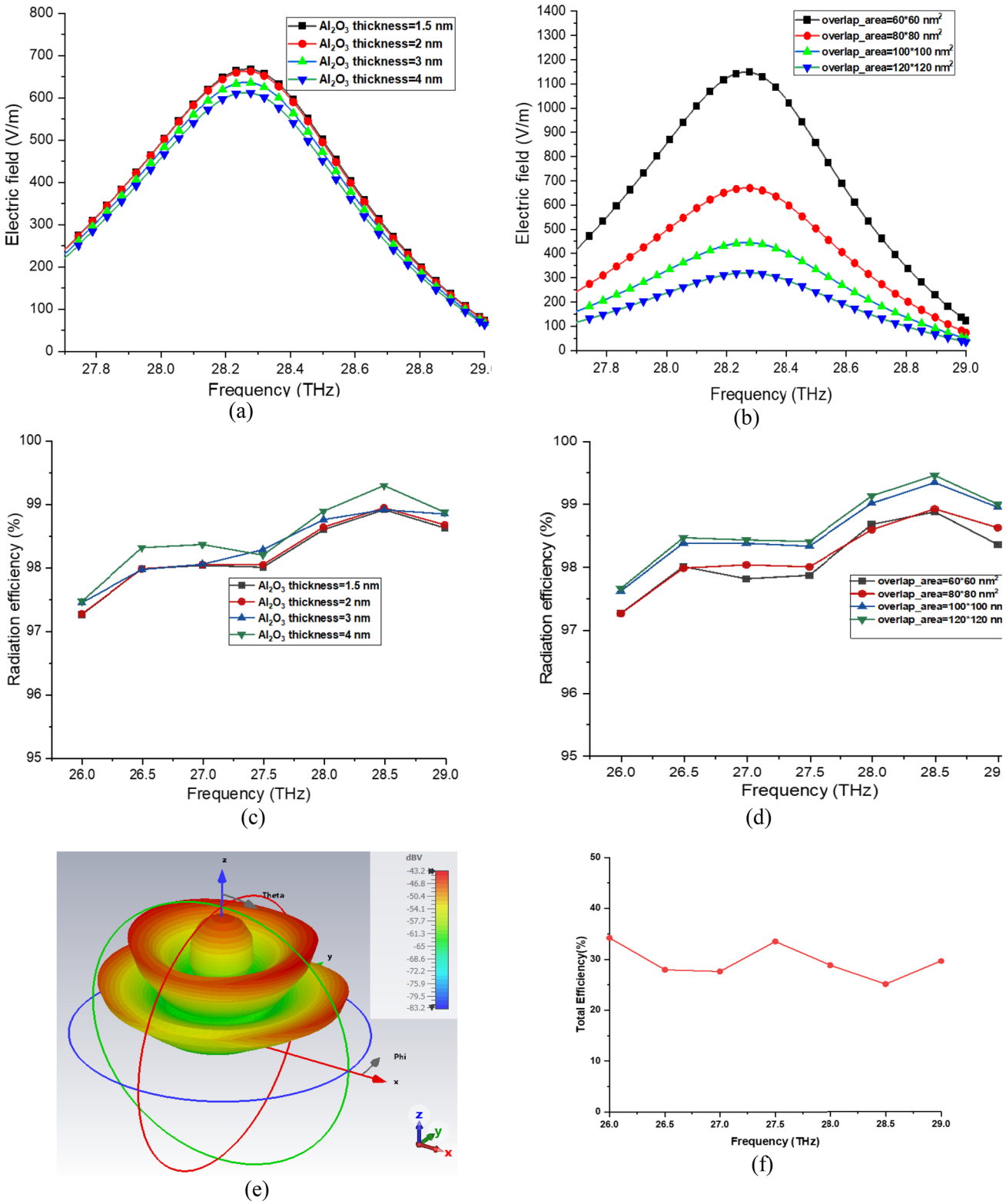


**Fig. 11** Electric field versus frequency for **a** Insulator thickness variation and **b** overlapping area variation. Radiation efficiency versus frequency for different values of **c** insulator thickness **d** overlapping area **e** 3D E-pattern of the overlap VSNA with insulator ($Al_2O_3$) at 28THz and **f** total efficiency of the VSNA with MIM diode

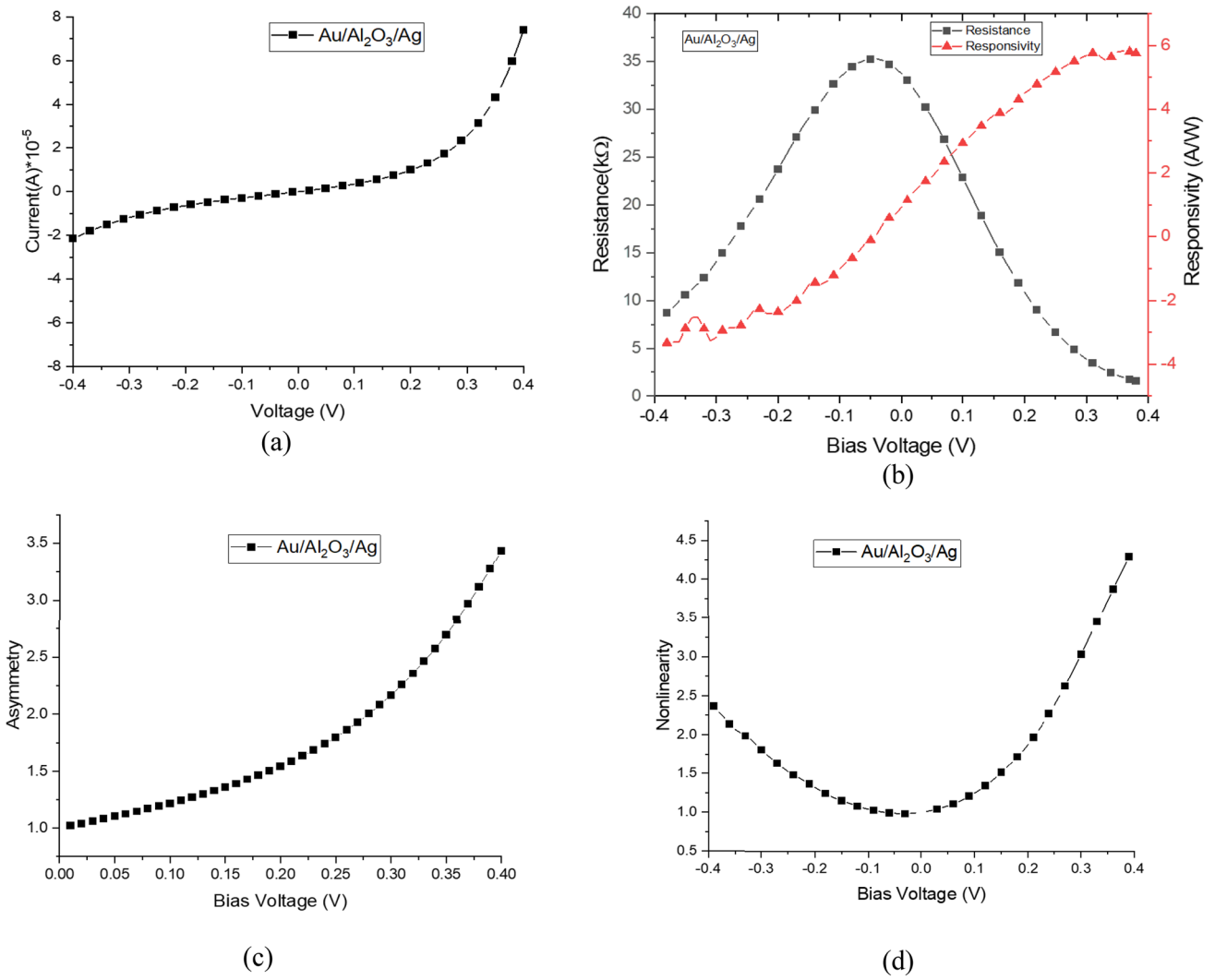


**Fig. 12** **a** *I-V* characteristic; **b** responsivity and dynamic resistance; **c** asymmetry; and **d** nonlinearity versus bias voltage

**Table 2** Figure of merits of MIM diodes using $Al_2O_3$ as an insulator compared with previous works at 28.3THz

| References | Antenna design | Diode | Resistance at zero bias (Ω) | Responsivity at zero bias (A/W) | Diode area ($nm^2$) | Efficiency (%) at 28.3 THz |
|---|---|---|---|---|---|---|
| [10] | Dipole | Al/ $Al_2O_3$/Ti | – | 0.6 | ~50*50 | – |
| | | Al/ $Al_2O_3$/Pt | – | 1 | | |
| | | Al/ $Al_2O_3$/Ni | – | 0.5 | | |
| [12] | Slot antenna-based FSS | Al/ $Al_2O_3$/Pt | 124 | $1.24*10^{-3}$ | ~80*100 | – |
| [13] | Bowtie | Au/$Al_2O_3$/Ti | 98 K | 0.44 | ~200*200 | 11 |
| [16] | Vivaldi | Au/$Al_2O_3$/Ti | $4*10^{11}$ | 1 | 200*210 | 10.82 |
| [15] | Log-spiral | Au/$Al_2O_3$/Cu | $3.5*10^{12}$ | 0.5 | 2*5 | – |
| | | Au/$Al_2O_3$/Cr | $2.5*10^{12}$ | 0.5 | | |
| | | Au/$Al_2O_3$/Ti | $1.2*10^{12}$ | 0.5 | | |
| | | Au/$Al_2O_3$/Al | $0.9*10^{12}$ | 0.5 | | |
| | | Au/$Al_2O_3$/Ag | $0.85*10^{12}$ | 0.5 | | |
| This work | V-shape | Au/$Al_2O_3$/Ag | 33.7 K | 0.93 | 60*60 | 26.58 |

## 5 Conclusion

In this paper, a potentially printable V-shaped nanoantenna (VSNA) has been designed, simulated, and compared to a conventional dipole with the same length, width, and thickness. The VSNA structure is based on a conventional dipole antenna, in which the two arms are close to each other at their apex, thus forming an angle β between them. The study has shown that the VSNA exhibits better and more localized field enhancement at the arm tips, with an improvement of more than 300% compared to a conventional dipole nanoantenna. An optimization has been performed to achieve maximum electric field and resonance at 28.3 THz by tilting the conventional dipole with an angle of 45° relative to the axis. It has been demonstrated that despite the dimension constraints, a resonant antenna can be printed by changing the orientation of each arm of the antenna. Then, the overlap structure of the two arms of the antenna with an insulator between them has shown a radiation efficiency of more than 98%. The reported design offers a total efficiency of 26.58% with an enhancement of 141% compared to the previous study, which had a radiation efficiency of 11%. Beyond the potentialities presented by the proposed design, its simplicity makes it manufacturable for potential energy harvesting applications. The MIM diode ($Au/Al_2O_3/Ag$) simulation has also shown a responsivity and dynamic resistance of 33.7 kΩ and 0.93 A/W at zero bias, respectively.

**Acknowledgements** This work was supported by the Partnership for Skills in Applied Sciences, Engineering and Technology (PASET)-Regional Scholarship and Innovation Fund (RSIF).

**Author contributions** Aboubacar, Uli, and Mohamed have proposed the idea. Aboubacar has done the simulations. All authors have contributed to the paper's analysis, discussion, writing, and revision.

**Funding** Open Access funding enabled and organized by Projekt DEAL. Open Access funding enabled and organized by Project DEAL.

**Data availability** No datasets were generated or analyzed during the current study.

## Declarations

**Conflict of interests** The authors declare no competing interests.

**Ethical approval** The authors would like to clarify that there is no financial/non-financial interests that are directly or indirectly related to the work submitted for publication.



## References

1. Zainud-Deen, S.H., Eltresy, N.A., Malhat, H.A., Awadalla, K.H.: Single/dual-polarized infrared rectenna for solar energy harvesting. Adv. Electromagn. **5**(2), 1 (2016)
2. Grover, S., Moddel, G.: Engineering the current-voltage characteristics of metal-insulator-metal diodes using double-insulator tunnel barriers. Solid State Electron. **67**(1), 94–99 (2012)
3. Kawase, K., Ogawa, Y., Minamide, H., Ito, H.: Terahertz parametric sources and imaging applications. Semicond. Sci. Technol. **20**(7), S258–S265 (2005)
4. Donchev, E., Technologies, L., Pang, J.S., Gammon, P.M., Centeno, A.E.R.: The rectenna device : from theory to practice (a review ). MRS Energy Sustain. (2014). https://doi.org/10.1557/mre.2014.6
5. Wang, Z., Hensleigh, R., Xu, Z., Wang, J., Park, J.J., Papathanasopoulos, A.: Ultra-light antennas via charge programmed deposition additive manufacturing. Nat. Commun. (2025). https://doi.org/10.1038/s41467-024-53513-w
6. Tütüncü, B., Türktam, U.: Microwave absorber surface design for 5G energy harvesting applications. Phys. Scr. **99**(11), 115503 (2024)
7. İmeci, T., Tütüncü, B., Herceg, L.: Performance-enhanced s-shaped slotted patch antenna for X Band/Ku band applications. Wirel. Pers. Commun. **129**(2), 1069–1082 (2023)
8. Shriwastava, S., Tripathi, C.C.: Metal–insulator–metal diodes: a potential high frequency rectifier for rectenna application. J. Electron. Mater. **48**(5), 2635–2652 (2019)
9. Ma, Z., Vandenbosch, G.A.E.: Optimal solar energy harvesting efficiency of nano-rectenna systems. Sol. Energy **88**, 163–174 (2013)
10. Esfandiari, P., et al.: Tunable antenna-coupled metal-oxide-metal (MOM) uncooled IR detector. Infrared Technol. Appl. XXXI **5783**, 470 (2005)
11. Gadalla, M.N., Abdel-Rahman, M., Shamim, A.: Design, optimization and fabrication of a 28.3â€...THz nano-rectenna for infrared detection and rectification. Sci. Rep. **4**, 1–9 (2014)
12. Kinzel, E.C., Brown, R.L., Ginn, J.C., Lail, B.A., Slovick, B.A., Boreman, G.D.: Design of an MOM diode-coupled frequency-selective surface. Microw. Opt. Technol. Lett. **55**(12), 2611–2615 (2013)
13. Jayaswal, G., Belkadi, A., Meredov, A., Pelz, B., Moddel, G., Shamim, A.: Optical rectification through an $Al_2O_3$ based MIM passive rectenna at 28.3 THz. Mater. Today Energy **7**, 1–9 (2018)
14. Hamied, F.M.A., Mahmoud, K.R., Hussein, M., Obayya, S.S.A.: Design and analysis of rectangular spiral nano-antenna for solar energy harvesting. Prog. Electromagn. Res. C **111**(January), 25–34 (2021)
15. Yahyaoui, A., Elsharabasy, A., Yousaf, J., Rmili, H.: Numerical analysis of MIM-based log-spiral rectennas for efficient infrared energy harvesting. Sensors (Switzerland) **20**(24), 1–16 (2020)
16. Amara, W., et al.: Vivaldi dipole nano-rectenna for IR energy harvesting at 28.3 THz. Int. J. Numer. Model. Electron. Netw., Devices Fields **34**(2), 1–13 (2021)

17. Khouqeer, G.A., et al.: A study on bowtie antenna based optical rectenna system for THz energy harvesting applications. Opt. Quantum Electron. **55**(8), 1–12 (2023)
18. Rashidi, A., Chryssomallis, M.T., Anagnostou, D.E.: Tailorable optical scattering properties of V-shaped plasmonic nanoantennas: a computationally efficient and fast analysis. J. Opt. Soc. Am. A **31**(10), 2256 (2014)
19. Jiao, J., et al.: Study on focusing properties of broadband range and oblique incidence on the basis of V-shaped nanoantenna. Appl. Phys. A Mater. Sci. Process. **122**(11), 1–6 (2016)
20. Gadalla, M.N., Abdel-Rahman, M., Shamim, A.: Design, optimization and fabrication of a 28.3THz nano-rectenna for infrared detection and rectification. Sci. Rep. **4**, 1–9 (2014)
21. González, F.J., Alda, J., Simón, J., Ginn, J., Boreman, G.: The effect of metal dispersion on the resonance of antennas at infrared frequencies. Infrared Phys. Technol. **52**(1), 48–51 (2009)
22. Chandra Paul, L.: The effect of changing substrate material and thickness on the performance of inset feed microstrip patch antenna. Am. J. Netw. Commun. **4**(3), 54 (2015)
23. Iluz, Z., Boag, A.: Wideband dual Vivaldi nano-antenna with high radiation efficiency over the infrared frequency band. In: 2011 IEEE International Conference on Microwaves, Communications, Antennas and Electronic Systems (COMCAS 2011), vol. 36, no. 15, pp. 1–3 (2011)
24. Hu, W., Sarveswaran, K., Lieberman, M., Bernstein, G.H.: Sub-10 nm electron beam lithography using cold development of poly (methylmethacrylate). J. Vac. Sci. Technol. B: Microelectron. Nanometer Struct. Process., Meas., Phenom. **22**(4), 1711–1716 (2004)
25. Lv, J.T., Yan, Y., Zhang, W.K., Liu, Y.H., Jiang, Z.Y., Si, G.Y.: Plasmonic nanoantennae fabricated by focused Ion beam milling. Int. J. Precis. Eng. Manuf. **16**(4), 851–855 (2015)
26. Abdel, F.M., Korany, H., Hussein, M., Obayya, S.S.A.: Design and analysis of a nano-rectenna based on multi-insulator tunnel barrier for solar energy harvesting. Opt. Quantum Electron. **54**, 144 (2022)
27. Yang, H.U., D'Archangel, J., Sundheimer, M.L., Tucker, E., Boreman, G.D., Raschke, M.B.: Optical dielectric function of silver. Phys. Rev. B–Condens. Matter Mater. Phys. **91**(23), 1–11 (2015)
28. Ordal, M.A., Bell, R.J., Alexander, R.W., Long, L.L., Querry, M.R.: Optical properties of fourteen metals in the infrared and far infrared: Al Co, Cu, Au, Fe, Pb, Mo, Ni, Pd, Pt, Ag, Ti, V, and W. Appl. Opt. **24**(24), 4493 (1985)
29. Liu, G., Zhao, C., Jiang, J., Gao, Z., Gu, J.: Structural design and optimization of optical nano-antenna based on bridge structure. Prog. Electromagn. Res. M **117**(May), 95–104 (2023)
30. Wiatrowska, A., et al.: Ultra-precise printing of micrometer-size interconnectors for high-resolution microled displays. Dig. Tech. Pap. - SID Int. Symp. **52**(1), 833–836 (2021)
31. Łysień, M., et al.: High-resolution deposition of conductive and insulating materials at micrometer scale on complex substrates. Sci. Rep. **12**(1), 1–18 (2022)
32. Biagioni, P., Huang, J.S., Hecht, B.: Nanoantennas for visible and infrared radiation. Rep. Prog. Phys. **75**(2), 024402 (2012)
33. Agrawal, A., Kriegel, I., Milliron, D.J.: Shape-dependent field enhancement and plasmon resonance of oxide nanocrystals. J. Phys. Chem. C **119**(11), 6227–6238 (2015)
34. Belkadi Dostart, A.: Metal-Insulator-Metal Diodes for Ambient Heat Harvesting With Rectennas. University of Colorado at Boulder ProQuest Dissertations Publishing, (2020)
35. Aydinoglu, F., Alhazmi, M., Cui, B., Ramahi, O.M., Irannejad, M., Yavuz, M.: Higher performance metal-insulator-metal diodes using multiple insulator layers. Austin J. Nanomed. Nanotechnol. **1**(1), 2–4 (2013)
36. Shanawani, M., Masotti, D., Costanzo, A.: THz rectennas and their design rules. Electronics **6**(4), 99 (2017)
37. Khan, A.A., Jayaswal, G., Gahaffar, F.A., Shamim, A.: Metal-insulator-metal diodes with sub-nanometre surface roughness for energy-harvesting applications. Microelectron. Eng. **181**, 34–42 (2017)